RKKY Ferromagnetism with Ising-Like Spin States in Intercalated $Fe_{1/4}TaS_2$

K.-T. Ko,[1] Kyoo Kim,[2] Sung Baek Kim,[3,4] H.-D. Kim,[2,5] J.-Y. Kim,[2,5] B. I. Min,[2] J.-H. Park,[1,5,6,*] F.-H. Chang,[7] H.-J. Lin,[7] A. Tanaka,[8] and S-W. Cheong[3,9]

[1]*c_CCMR & Department of Physics, Pohang University of Science and Technology, Pohang 790-784, Korea*
[2]*Department of Physics, Pohang University of Science and Technology, Pohang 790-784, Korea*
[3]*l_PEM & Department of Physics, Pohang University of Science and Technology, Pohang 790-784, Korea*
[4]*Advancement for College Education Center, Konyang University, Chungnam 320-711, Korea*
[5]*Pohang Accelerator Laboratory, Pohang University of Science and Technology, Pohang 790-784, Korea*
[6]*Division of Advanced Materials Science, Pohang University of Science and Technology, Pohang 790-784, Korea*
[7]*National Synchrotron Radiation Research Center, Hsinchu 30077, Taiwan*
[8]*Department of Quantum Matter, ADSM, Hiroshima University, Higashi-Hiroshima 739-8526, Japan*
[9]*R-CEM & Department of Physics and Astronomy, Rutgers University, Piscataway, New Jersey 08854, USA*

(Received 2 March 2011; published 7 December 2011)

We investigated the magnetic nature of $Fe_{1/4}TaS_2$ using x-ray absorption spectroscopy, photoemission spectroscopy, and first principles band calculations. The results show a large unquenched orbital magnetic moment ($\sim 1.0\ \mu_B$/Fe) at intercalated Fe sites, resulting in a gigantic magnetic anisotropy ($H_A \simeq 60$ T). The magnetic coupling is well understood in terms of the Ruderman-Kittel-Kasuya-Yosida (RKKY) interaction, suggesting a novel RKKY ferromagnet with Ising-type spin states. We also found that this indirect exchange coupling between the neighboring Fe spins is ferromagnetic and maximized at the Fe-Fe distance of 2×2 superstructure.

DOI: 10.1103/PhysRevLett.107.247201 PACS numbers: 75.30.Gw, 71.20.−b, 78.70.Dm, 79.60.−i

Since the discovery of new physics on graphene and topological insulators, systems with hexagonal layers bound by van der Waals bonding have been refocused in the condensed matter physics society. Transition metal dichalcogenide MX_2 (M = transition metal and X = S, Se, Te), one of such systems, which shows the charge density wave phenomena [1,2], is another candidate for the appearance of interesting novel physical properties. The allowance of the intercalation of magnetic ions or molecules between the layers [1] provides us a new playground for emerging electrical and magnetic phenomena including superconductivity [3,4] and magnetism [5–7].

Fe_xTaS_2, a 2H-TaS_2 based magnetic ion intercalated transition metal dichalcogenide [5,6], exhibits interesting magnetic behaviors with a ferromagnetic (FM) to antiferromagnetic (AFM) transition at $x \simeq 0.4$ [8,9]. In the FM region ($x < 0.4$), the Curie temperature T_C strongly varies with the Fe concentration x. As x increases, T_C increases to reach a maximum $T_C \simeq 160$ K at $x = 1/4$ and then decreases to $T_C \simeq 35$ K at $x = 1/3$. Interestingly, the intercalated irons were found to form 2×2 or $\sqrt{3} \times \sqrt{3}$ superstructures at $x = 1/4$ or $1/3$, respectively [5,10,11] [see Fig. 1(a)]. The 2×2 superlattice intimately involves the highest T_C, and its disturbance suppresses T_C drastically [11]. Furthermore, $Fe_{1/4}TaS_2$ displays a variety of exotic magnetic properties such as a sharp switching of magnetization, an extremely large magnetocrystalline anisotropy, anisotropic magnetoresistance, and the anomalous Hall effect [10,12]. As shown in Fig. 1(b), the magnetic hysteresis along the c axis shows good squareness with a saturation moment $M_{\mathrm{sat}} \simeq 4\mu_B$/Fe while the in-plane moment is barely magnetized even at a high magnetic field of 6 T [11]. The anisotropy field was estimated to be $H_A \simeq 60$ T [10,11] from extrapolation, which is even much larger than that of rare-earth hard magnets [13]. On the other hand, the RKKY interaction was considered as the exchange mechanism for the magnetic ordering of far separated Fe^{2+} ions in this system [5,7]. However, due to lack of detailed electronic structure studies, the understanding is very limited, and clear explanations for the magnetic properties and exchange mechanism have never been made.

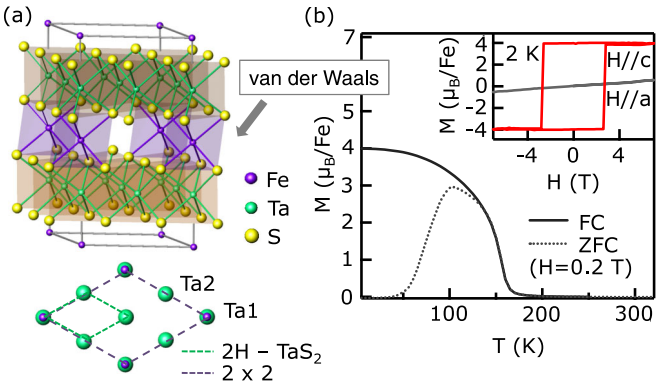

FIG. 1 (color online). (a) Crystal structure of $Fe_{1/4}TaS_2$. The lower panel shows the 2×2 superstructure formed by the intercalated Fe. (b) Field cooled (FC) and zero field cooled (ZFC) M-T curves under $H = 0.2$ T along the c axis. The in-plane ($H \parallel a$) and out-of-plane ($H \parallel c$) M-H hysteresis curves at 2 K are presented in the inset.

In this Letter, we report RKKY ferromagnetism with Ising-type spin states as the magnetic nature of $Fe_{1/4}TaS_2$ based on detailed electronic information obtained from comprehensive spectroscopic and theoretical studies including the Fe $L_{2,3}$-edge x-ray absorption spectroscopy (XAS), x-ray magnetic circular dichoism (XMCD), angle resolved photoemission spectroscopy (ARPES), many-body model calculations, and first principles band calculations. An extremely large orbital magnetic moment ($m_o \simeq 1.0\ \mu_B$/Fe), which persists at the intercalated Fe^{2+} ion and originates the gigantic magnetocrystalline anisotropy, agrees with H_A and brings on the Ising-type spin states. We found that the Fermi momentum k_F determined from ARPES resonates at the 2×2 superstucture to maximize the FM RKKY interaction, i.e., the maximum T_C. M_{sat} as well as the unquenched large m_o were also confirmed in theoretical studies of both the many-body cluster model calculation and the density functional theory within the generalized gradient approximation including the Coulomb correlation correction and spin-orbit coupling (GGA + U + SOC).

High quality $Fe_{1/4}TaS_2$ single crystals grown by a chemical vapor transport method [8,11] were checked with the x-ray diffraction [14], and the sharp 2×2 superlattice peak was confirmed [11]. The measurements were carried out at the 11A (XAS/XMCD) beam line in NSRRC, Taiwan and the 2A (XAS/XMCD) and 3A1 (ARPES) beam lines in PLS, Korea. The samples were cleaved *in situ* in ultrahigh vacuums better than 1×10^{-9} Torr (XAS/XMCD) and 1×10^{-10} Torr (ARPES). All the spectra were measured at 80 K. The $\vec{E} \parallel \vec{c}$ and $\vec{E} \perp \vec{c}$ XAS spectra were obtained at 70° and 0° incident angles to the c axis, respectively [15]. The XMCD measurements were performed with ~80% circularly polarized light at 27.5° incident angle to the c axis, and a 1 T electromagnet was used for the magnetization switch along the c axis [15]. The XAS/XMCD spectra were collected in the total electron yield mode. The ARPES spectra were collected with 20 meV total energy resolution by using SCIENTA SES-2002 electron analyzers. The Fermi surface map was obtained by integration of ±50 meV at $h\nu = 54.5$ eV. The GGA + U + SOC calculations were performed by using the full potential linearized augmented plane wave band method implemented in the WIEN2K code [16] with $34 \times 34 \times 16$ **k**-points in the full Brillouin zone.

Figure 2 shows the Fe L-edge XMCD and XAS results. The spectra are divided into the L_3 ($2p_{3/2}$) and L_2 ($2p_{1/2}$) regions due to the large $2p$ core hole spin-orbit coupling energy. In XMCD, the absorption spectra ρ_+ and ρ_- were collected for the magnetization parallel and antiparallel to the photon helicity vector, respectively. From the integration $\Sigma(\Delta\rho)$ in Fig. 2(a), we obtained $p = -1.46$ and $q = -1.10$ integration values over the L_3 and entire $L_{2,3}$ regions, respectively. The equal sign of the p and q values implies that the spin and orbital moments are parallel to each other, reflecting the more than half full Fe^{2+} (d^6) configuration. One notes that the q value, which is proportional to m_o, is far from zero. From the p and q values, the orbital to spin moment ratio is estimated to be $m_o/m_s = 0.33$ in the sum rule [17]. In the ionic spin moment ($4\mu_B$) limit, this ratio yields quite large $m_o = 1.33\mu_B$, which is reduced considerably in the real system due to the covalency and band formation.

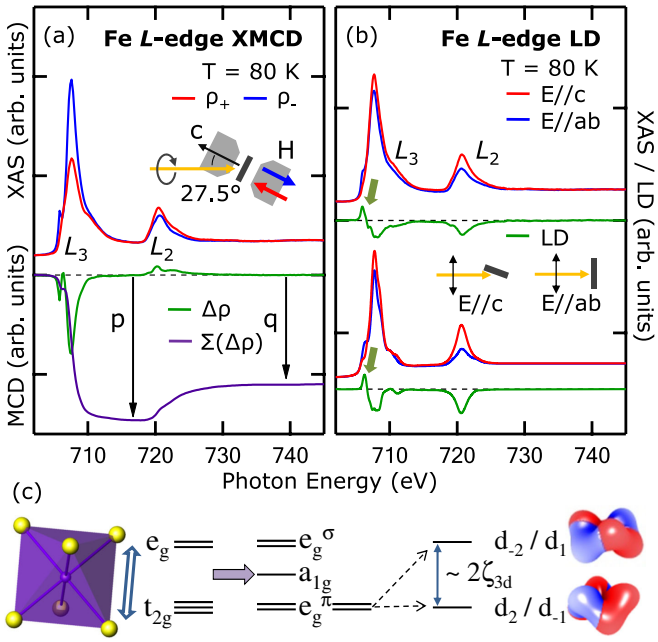

FIG. 2 (color online). (a) Fe L-edge XMCD results of $Fe_{1/4}TaS_2$ at 80 K. p and q correspond to the integration values over the L_3 and $L_{2,3}$ regions of the MCD spectrum $\Delta\rho$, respectively. (b) The polarization dependent XAS spectra (top) compared with the cluster model calculation results (bottom). The thick arrows point the transition to the in-plane orbitals. (c) Schematic diagrams of the orbital level splittings by the crystal field (left) and the spin-orbit coupling (right). The large unquenched m_o resides in the lowest state (d_2, d_{-1}) split from the low lying e_g^π orbital.

To examine orbital occupation producing the large m_o value, we measured the polarization dependent Fe $L_{2,3}$-edge XAS spectra, $\rho(\vec{E} \perp \vec{c})$ and $\rho(\vec{E} \parallel \vec{c})$, which show considerable difference involving orbital anisotropy. As shown in Fig. 2(b), the linear dichroism (LD) $\rho(\text{LD}) = \rho(\vec{E} \perp \vec{c}) - \rho(\vec{E} \parallel \vec{c})$ is overall negative in the Fe L-edge region except the L_3-edge leading part, indicating more $3d$ holes along the c axis. Positive signals in this leading part indicate that the unoccupied lowest energy state has the in-plane orbital character d_{xy} and $d_{x^2-y^2}$, as explained with crystal field splittings in Fig. 2(c) [18]. The distorted FeS_6 octahedron in $Fe_{1/4}TaS_2$ has D_{3d} trigonal site symmetry, and the $3d$ levels are split into e_g^π, a_{1g}, and e_g^σ levels. The lowest e_g^π doublet corresponds to $|e_g^{\pi 1}\rangle = -a|d_{x^2-y^2}\rangle + ib|d_{yz}\rangle$ and $|e_g^{\pi 2}\rangle = -ia|d_{xy}\rangle - b|d_{zx}\rangle$ ($a = \sqrt{\frac{2}{3}}$ and $b = \sqrt{\frac{1}{3}}$

in an ideal octahedron). Here the coefficient a increases with the elongated trigonal distortion, and the e_g^π states contain more in-plane d_{xy} and $d_{x^2-y^2}$ characters. Thus an additional minority spin electron occupies one of the e_g^π states to give a $|3d_\uparrow^5(e_g^\pi)_\downarrow^1\rangle$ configuration state so that the Fe^{2+} ion has more holes along the c axis (z axis) while the lowest unoccupied e_g^π orbital has more in-plane characters, in good agreement with the observed LD features. One notes that the e_g^π doublet consisting of $d_{\pm 2}$ and $d_{\pm 1}$ atomic orbitals can be split by the spin-orbit coupling as schematically described in Fig. 2(c). Then this additional splitting lowers the d_2/d_{-1} orbital resulting in the large unquenched m_o in $Fe_{1/4}TaS_2$.

For quantitative understanding, we mimicked the polarization dependent XAS spectra using the cluster model calculations [19] for the trigonal elongated FeS_6 [10]. As can be seen in the bottom of Fig. 2(b), the calculated spectra well reproduce the measured ones including the L_3 leading part as well as the overall LD features. The calculations, which also well reproduce the XMCD spectra [14], show that the occupied minority spin states have a 3:1 in-plane $d_{xy}/d_{x^2-y^2}$ to out-of-plane d_{yz}/d_{zx} character. The expectation values were estimated to be $m_s = 3.74\mu_B$ and $m_o = 1.46\mu_B$ with $m_o/m_s = 0.39$ close to the observed value 0.33 in XMCD. However, the estimated total moment $m_{\rm tot} = 5.20\mu_B$ is about 30% larger than the observed $M_{\rm sat} \simeq 4.0\mu_B$. In the sulfides, valence electrons have more bandlike characters than those in the oxides, and the local cluster model calculation naturally overestimates the real moment [20].

To elucidate the full electronic structure of $Fe_{1/4}TaS_2$, we performed the GGA + U + SOC calculations with a reasonable Hubbard U-value (the Coulomb energy $U = 4.5$ eV and Hund exchange parameter $J_H = 0.7$ eV) for the Fe $3d$. The Fe $3d$ partial density of states (PDOS) in Figs. 3(a)–3(c) show that the majority spin states (red lines ↑) are mostly occupied, consistently with the high spin Fe^{2+}. In the minority spin states (blue lines ↓), the $d_{3z^2-r^2}$ occupation is negligible while $d_{xy}/d_{x^2-y^2}$ and d_{zx}/d_{yz} are partially occupied. Further, occupied $d_{xy}/d_{x^2-y^2}$ and d_{zx}/d_{yz} turn out to be nearly the d_2 and d_{-1} atomic orbital states, respectively. These results are in good agreement with the ionic picture of the lowest spin-orbit split orbital d_2/d_{-1} [Fig. 2(c)]. The calculation yields $m_s = 2.95\mu_B$ and $m_o = 1.00\mu_B$ at the Fe site, which is also consistent with the observed ratio $m_o/m_s = 0.33$. On the other hand, this large m_o causes a large magnetocrystalline anisotropy (MCA) energy ($E_{\rm MCA} \sim 15$ meV) involving $\Delta\vec{L}\cdot\vec{S}$ [21,22] and a huge $H_A \simeq 60$ T ($\vec{m}\cdot\vec{H}_A \sim 14$ meV) in $Fe_{1/4}TaS_2$. As a result of the large $E_{\rm MCA}$, the Fe^{2+} spins behave like Ising-types as those in $LuFe_2O_4$ [21,23] and $FeCl_2$ [24]. These Ising-type spin states are responsible for the sharp magnetization switching and large coercivity.

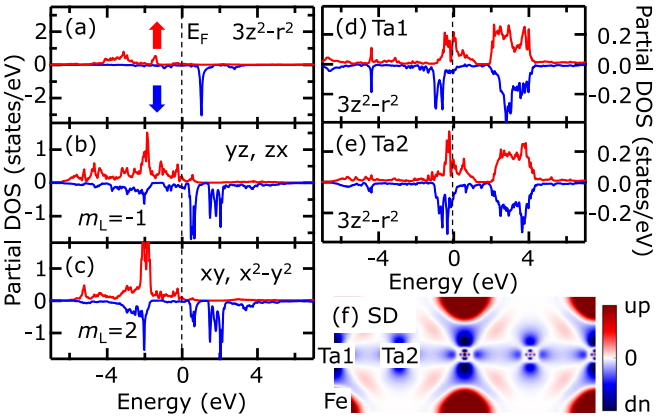

FIG. 3 (color online). (a)–(c) Fe $3d$ PDOS for majority (red ↑) and minority (blue ↓) spins from GGA + U + SOC. The occupied d_{yz}/d_{zx} and $d_{xy}/d_{x^2-y^2}$ correspond to the atomic d_{-1} and d_2, respectively. (d)–(e) Ta $5d_{3z^2-r^2}$ PDOS of Ta1 and Ta2 sites (see text). (f) Real space spin density in the (100) slice possessing the intercalated Fe, which visualizes the AFM coupling between Fe and Ta spin moments.

In addition, the calculations show that Ta $5d_{3z^2-r^2}$ bands are also spin polarized due to AFM coupling with Fe $3d$ ones although the induced moment is tiny as shown in Figs. 3(d) and 3(e). The estimated moments are $-0.071\mu_B$ at the Ta1 site on the intercalated Fe ion and $-0.033\mu_B$ at the Ta2 site on the empty site [see Fig. 1(a)]. The relatively large moment at the Ta1 site is due to its tight coupling to the magnetic Fe. These unequal moments lead the $5d_{z^2}$ spin density modulation with a period of $2a$, which is the same as the one of the intercalated Fe in $Fe_{1/4}TaS_2$ shown in Fig. 4(f). Additional moments, which are induced at the S sites mainly due to the Fe $3d$-S $3p$ hybridization, are estimated to be $0.028\mu_B$/S for the

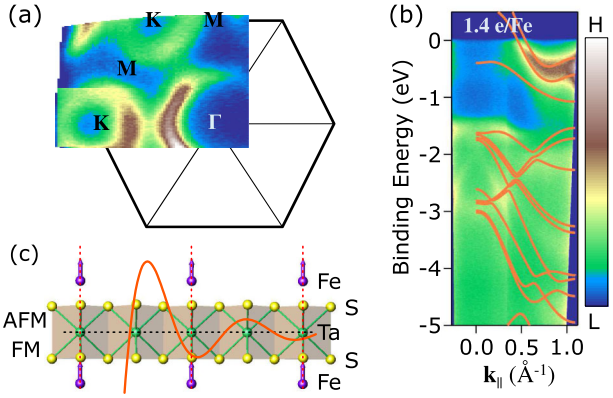

FIG. 4 (color online). (a) ARPES intensity map at E_F of $Fe_{1/4}TaS_2$, which shows hole pockets around Γ and K-points in the 1st Brillouin zone (bold solid). (b) ARPES results along $\overline{\Gamma M}$ compared with the theoretical band dispersion (solid lines) of 2H-TaS_2 with -0.2 eV shift (1.4 electrons/Fe doping). (c) Real space RKKY oscillation curve in the (001) slice as in Fig. 3(f) with $k_F = 0.53$ Å^{-1}.

neighboring S ions and $0.005\mu_B$/S for the others. The total moment is obtained to be $3.94\mu_B$ per $FeTa_4S_8$ which agrees well with the observed $M_{sat} \simeq 4.0\mu_B$.

The tight Fe-Ta AFM interaction binds Fe ions ferromagnetically along the c axis, and reduces the system to an effective two dimensional magnetic system of far separated magnetic Fe chains interacting through itinerant Ta $5d$ electrons. Thus, we performed ARPES to explore the electronic structure of the Ta $5d$ bands, which gives a clue for the RKKY magnetic exchange interaction in $Fe_{1/4}TaS_2$. Figure 4(a) shows Fermi surface (FS) topology of $Fe_{1/4}TaS_2$, which consists of two hole pockets around Γ- and K-points similar to that of the undoped 2H-TaS_2 [25,26] except for somewhat shrunken hole pockets. As shown in Fig. 4(b), the band dispersions obtained from the ARPES measurements also agree well with the theoretical ones of 2H-TaS_2 along $\overline{\Gamma M}$ after a 0.2 eV rigid band shift, despite the small difference in the S $3p$ band dispersion. These results indicate that the Fe $3d$-S $3p$ hybridization is relatively weak and the intercalated Fe acts like an electron donor. We also confirmed that the measured FS agrees well with the FS obtained from the GGA + U + SOC results of the $Fe_{1/4}TaS_2$ supercell when the Brillouin zone folding involving the 2×2 superstucture is implemented [14]. The 0.2 eV shift corresponds to a 1.4 electron doping per Fe, which is somewhat smaller than the 2 electrons/Fe doping expected for ionic Fe^{2+}. This is mainly due to the covalence of Fe $4sp$-S $3sp$ bonding as predicted in the calculation.

From the ARPES results, we extracted $k_F \simeq 0.53$ Å^{-1} along $\overline{\Gamma K}$ [27], and estimated the RKKY exchange interaction as a function of the interstitial distance [28] shown in Fig. 4(c). The ferromagnetic exchange interaction becomes maximized at the Fe-Fe distance of the 2×2 superstucture to yield the maximum T_C at $x = 0.25$ in Fe_xTaS_2. The coupling is still FM for smaller Fe concentrations ($x \sim 0.2$). For $x > 0.25$, T_C decreases as x increases, and eventually the coupling becomes AFM [8,9]. The RKKY oscillation [Fig. 4(c)] shows that the coupling varies as a function of the k_F and Fe-Fe distance. But considering that T_C is suppressed even by simple disturbance of the superstructure in $Fe_{1/4}TaS_2$, the population of the 2×2 superstructure may also affect the exchange interaction.

In conclusion, we report the magnetic nature of $Fe_{1/4}TaS_2$ based on the various experimental and theoretical results. The results manifest that $Fe_{1/4}TaS_2$ is a RKKY ferromagnet with Ising-type spin states. A large unquenched m_o is sustained at the intercalated Fe and the local Fe spins are aligned ferromagnetically through itinerant Ta $5d$ electrons. We also found that the 2×2 superstructure is crucial to obtain a high T_C value. These findings can be transferred to magnetism studies in other hexagonal layered systems including graphene and topological insulators [29].

We thank Jae Hoon Kim for the optical measurements. This work was supported by the National Creative Initiative Project No. 2009-0081576, WCU Program No. R31-2008-000-10059-0, Leading Foreign Research Institute Recruitment Program No. 2010-00471, and Grant No. 2009-0079947 (B. I. M.) and No. 2011-0006408 (S. B. K) through NRF funded by MEST. PAL is supported by POSTECH and MEST.

*Author to whom all correspondence should be addressed. jhp@postech.ac.kr

[1] J. A. Wilson and A. D. Yoffe, Adv. Phys. **18**, 193 (1969).
[2] J. A. Wilson, F. J. Di Salvo, and S. Mahajan, Adv. Phys. **24**, 117 (1975).
[3] K. E. Wagner *et al.*, Phys. Rev. B **78**, 104520 (2008).
[4] R. M. Fleming and R. V. Coleman, Phys. Rev. Lett. **34**, 1502 (1975).
[5] S. S. P. Parkin and R. H. Friend, Philos. Mag. B **41**, 65 (1980).
[6] S. S. P. Parkin and R. H. Friend, Philos. Mag. B **41**, 95 (1980).
[7] R. H. Friend, A. R. Beal, and A. D. Yoffe, Philos. Mag. **35**, 1269 (1977).
[8] M. Eibschütz *et al.*, J. Appl. Phys. **52**, 2098 (1981).
[9] H. Narita *et al.*, J. Solid State Chem. **108**, 148 (1994).
[10] E. Morosan *et al.*, Phys. Rev. B **75**, 104401 (2007).
[11] Y. J. Choi *et al.*, Europhys. Lett. **86**, 37012 (2009).
[12] J. G. Checkelsky *et al.*, Phys. Rev. B **77**, 014433 (2008).
[13] H. R. Kirchmayr, J. Phys. D **29**, 2763 (1996).
[14] See Supplemental Material at http://link.aps.org/supplemental/10.1103/PhysRevLett.107.247201 for the x-ray diffraction patterns (Fig. S1), the theoretical XMCD spectra (Fig. S2), or the calculated Fermi surface of the supercell (Fig. S3).
[15] Because of the imperfection geometry and 80% circular polarization, the linear dichroism and MCD reflect 88% and 63% in the intensity, respectively.
[16] P. Blaha *et al.*, *WIEN2K, An Augmented Plane Wave + Local Orbitals Program for Calculating Crystal Properties* (Vienna University of Technology, Vienna, Austria, 2001).
[17] B. T. Thole, P. Carra, F. Sette, and G. van der Laan, Phys. Rev. Lett. **68**, 1943 (1992); C. T. Chen *et al.*, *ibid.* **75**, 152 (1995).
[18] S. Sugano, T. Tanabe, and H. Kamimura, *Multiplets of Transition-Metal Ions in Crystals* (Academic Press, New York, USA, 1970).
[19] A. Tanaka and T. Jo, J. Phys. Soc. Jpn. **63**, 2788 (1994). The calculations were performed for $d^n \bigoplus d^{n+1}\underline{L} \bigoplus d^{n+2}\underline{L}^2$. The fitting parameters are Coulomb $U_{dd} = 6.0$ eV, charge transfer energy $\Delta = 5.0$ eV, hybridization $(pd\sigma) = -1.4$ eV, and Slater integrals are ~72% of the atomic Hartree-Fock values.
[20] K. Shimada *et al.*, Phys. Rev. B **57**, 8845 (1998).
[21] K.-T. Ko *et al.*, Phys. Rev. Lett. **103**, 207202 (2009).

[22] G. van der Laan, J. Phys. Condens. Matter **10**, 3239 (1998); The magnetic anisotropy energy is determined by $\delta E \sim -\frac{1}{4}\zeta_{3d}\hat{S}\cdot\Delta L$, where $\Delta L = L_c - L_{ab} \simeq 0.8$ is the orbital momentum anisotropy obtained from the calculation.
[23] W. Wu *et al.*, Phys. Rev. Lett. **101**, 137203 (2008).
[24] P. Carrara, J. de Gunzbourg, and Y. Allain, J. Appl. Phys. **40**, 1035 (1969); P. Wong *et al.*, Phys. Rev. Lett. **55**, 2043 (1985).
[25] G. Wexler and A. M. Woolley, J. Phys. C **9**, 1185 (1976).
[26] P. Blaha, J. Phys. Condens. Matter **3**, 9381 (1991).
[27] The k_F value is consistent not only with the band calculations [14] but also with the plasma frequency ω_p in the optical measurements, which give information on the charge carrier density. We obtained $\omega_p \simeq 3.7$ eV in $Fe_{1/4}TaS_2$, which is about 20% larger than that of 2H-TaS_2.
[28] D. N. Aristov, Phys. Rev. B **55**, 8064 (1997).
[29] L. Brey, H. A. Fertig, and S. Das Sarma, Phys. Rev. Lett. **99**, 116802 (2007); Y. L. Chen *et al.*, Science **329**, 659 (2010); D. A. Abanin and D. A. Pesin, Phys. Rev. Lett. **106**, 136802 (2011).